Soft Matter

Cite this: *Soft Matter*, 2011, **7**, 2076

www.rsc.org/softmatter

PAPER

Brownian motion in a Maxwell fluid

Matthias Grimm,[abc] Sylvia Jeney[ab] and Thomas Franosch*[cd]

Received 6th July 2010, Accepted 8th November 2010
DOI: 10.1039/c0sm00636j

The equilibrium dynamics of a spherical particle immersed in a complex Maxwell fluid is analyzed in terms of velocity autocorrelation function (VACF), mean-square displacement (MSD), and power spectral density (PSD). We elucidate the role of hydrodynamic memory and its interplay with medium viscoelasticity for a free and a harmonically confined particle. The elastic response at high frequencies introduces oscillations in the VACF, which are found to be strongly damped by the coupling to the fluid. We show that in all Maxwell fluids hydrodynamic memory eventually leads to a power-law decay in the VACF as is already known for Newtonian fluids. The MSD displays asymptotically an intermediate plateau reflecting the elastic restoring forces of the medium. In the frequency domain, the PSD exhibits at high frequencies a step due to the trapping, whereas the low-frequency decay reflects the viscoelastic relaxation. Our results suggest that high-frequency microrheology is well-suited to infer the elastic modulus, which is sensitive over a wide range of Maxwell times.

1. Introduction

Soft matter, like emulsions, polymer solutions and biological fluids, displays viscoelastic properties, characterized by a complex frequency-dependent elastic modulus, that covers a broad spectrum of relaxation times. Whereas the low-frequency regime is typically studied by macrorheological methods,[1] the high-frequency regime is better accessed by microrheology.[2,3] The basic principle of microrheology is to use mesoscopic spherical particles immersed in a viscoelastic medium as local probes, and track their Brownian trajectories with high temporal and spatial resolution by light scattering[4,5] and/or video microscopy.[6] When only a single particle is tracked, the particle is better held by an optical trap, which provides a light source for position tracking, and ensures that it remains within the detection range.[7,8] Both, passive microrheology, where the displacement of the bead is due to thermal fluctuations only, as well as active microrheology, where external forces are exerted on the particle, for example by an optical trap, have been successfully applied.[9–11] Any deviation from the normal diffusive behavior of the particle is then interpreted as a response to the material properties of its complex environment.[12] In particular, the probe's Brownian motion is expected to be affected differently by a more or less viscous and/or elastic behavior of the surrounding medium. Typically, a generalized Stokes–Einstein relation[5,13] is employed to convert the mean-square displacement of the bead into the complex elastic modulus, $G(\omega) = G'(\omega) - iG''(\omega)$ of the fluid. This approach has revealed power-law behavior $G(\omega)\sim\omega^{\alpha}$ with $\alpha \approx 3/4$, for a variety of biological materials,[14] which has been identified as a fingerprint of the dynamics of single semi-flexible polymers.[15] However, the observation of the microrheological probe at short timescales, or equivalently at high frequencies, requires disentangling the frequency-dependent elastic modulus or the corresponding dynamic viscosity $\eta(\omega) := G(\omega)/(-i\omega)$ from the hydrodynamic memory induced by momentum conservation.[16] Indeed, at high frequencies, the viscous drag acting on the probe is retarded due to vortex diffusion and inertia of the particle, resulting in additional hydrodynamic memory. In a purely viscous fluid, this memory effect manifests itself as a long-time tail in the velocity autocorrelation function (VACF),[17,18] which was discovered first in computer simulations,[19] but was anticipated earlier also for colloidal single particle motion.[20,21] Indirect experimental evidence for the hydrodynamic memory was collected by diffusing-wave spectroscopy on dense colloidal suspensions,[22] yet the first direct observation was achieved only recently with high-precision optical trapping interferometry.[23,24] Similarly, by monitoring the correlated fluctuations of two optically trapped particles, the characteristic spatial backflow pattern associated with momentum conservation in the fluid[16,25] was measured directly. When considering such hydrodynamic contributions, a direct estimation of the complex modulus by Mason's method of taking logarithmic derivatives[13] no longer applies, and an improved algorithm based on Padé approximants in the Laplace domain was proposed recently by Felderhof.[26] Nevertheless,

[a]*Institut de Physique de la Matière Condensée, Ecole Polytechnique Fédérale de Lausanne (EPFL), CH-1015 Lausanne, Switzerland*
[b]*Biozentrum der Universität Basel, Klingelbergstrasse 50/70, CH-4056 Basel, Switzerland*
[c]*Arnold Sommerfeld Center for Theoretical Physics, Fakultät für Physik, Ludwig-Maximilians-Universität München, Theresienstraße 37, 80333 Munich, Germany. E-mail: franosch@physik.uni-erlangen.de*
[d]*Institut für Theoretische Physik, Universität Erlangen-Nürnberg, Staudtstraße 7, 91058 Erlangen, Germany*

a systematic study on the expected interplay of viscoelasticity and hydrodynamic memory is still lacking.

In this paper, we investigate the dynamics of a Brownian particle immersed in a simple viscoelastic fluid, and held by a weak harmonic potential as present in optical trapping experiments (Fig. 1). The simplest case for a viscoelastic fluid is provided by the Maxwell model,[27,28] which allows for a complete analytical description of the Brownian probe's dynamics in the case of instantaneous hydrodynamic friction. A Maxwell fluid displays a characteristic timescale τ_M that marks the transition from a high-frequency elastic regime to a purely viscous fluid at low frequencies. As Maxwell fluids already encode many of the generic aspects relevant to the description of fluids displaying frequency-dependent moduli, we expect our results to represent a reference case for more complex colloidal, polymeric or biological solutions. Rheological measurements of microemulsions, transient polymer networks, worm-like and giant micelle solutions[29–34] suggest Maxwell's model as a valid description of such fluids.

In the following, we first briefly recall how hydrodynamic memory is incorporated into the theory of Brownian motion (Sec. 2). Then the viscoelastic properties of a Maxwell fluid are discussed in Sec. 3. The main results for the VACF of the bead, the mean-square displacement (MSD) and the power spectral densities (PSD) of the displacements are presented for free Brownian motion in Sec. 4, and in the presence of harmonic restoring forces in Sec. 5. Finally, we summarize our results and discuss implications on microrheological studies in the high-frequency regime.

2. Brownian motion in a Newtonian fluid

Since the individual trajectory of a particle performing Brownian motion is unpredictable, a theoretical description of the dynamics aims at statistical properties such as correlation functions. Of particular interest is the velocity autocorrelation function (VACF), $C(t) := \langle v(t)v(0)\rangle$, which encodes also the mean-square displacement (MSD), $\delta x^2(t) := \langle [x(t) - x(0)]^2\rangle$ of one cartesian component through[27]

$$\delta x^2(t) = 2\int_0^t (t-t')C(t')\mathrm{d}t'. \tag{1}$$

In equilibrium, correlation functions are related to the deterministic linear response *via* the well-known fluctuation-dissipation theorem (FDT).[35] The macroscopic transport coefficient is the complex admittance $\mathscr{Y}(\omega)$, which relates the particle's velocity $v(\omega) = \mathscr{Y}(\omega)f(\omega)$ to a force $f(\omega)$ in the frequency domain. Hence the admittance is the frequency-dependent generalization of the Stokes' mobility in the steady case. Application of the FDT yields

$$C(\omega) = k_B T\mathscr{Y}(\omega), \tag{2}$$

where $C(\omega)$ is the one-sided Fourier transform of $C(t)$:

$$C(\omega) = \int_0^\infty \mathrm{e}^{\mathrm{i}\omega t}C(t)\mathrm{d}t. \tag{3}$$

For an incompressible fluid and no-slip boundary conditions at the surface of the Brownian particle, the force in response to unsteady motion is known as Boussinesq–Basset force[36–38] and the admittance follows as

$$\mathscr{Y}(\omega) = \frac{1}{-\mathrm{i}\omega m^* + \zeta(\omega)}. \tag{4}$$

The effective mass $m^* = m_p + m_f/2$ accounts for the inertial force due to acceleration of the particle's mass m_p and of the displaced fluid mass $m_f = 4\pi\rho_f a^3/3$. The frequency-dependent friction coefficient $\zeta(\omega)$ includes the hydrodynamic backflow effects

$$\zeta(\omega) = 6\pi\eta a\left[1 + \sqrt{-\mathrm{i}\omega\rho_f a^2/\eta}\right] \tag{5}$$

$$= \frac{m^*}{\tau_p^*}\left[1 + \sqrt{-\mathrm{i}\omega\tau_f}\right], \tag{6}$$

where a denotes the radius of the spherical particle, ρ_p its density, η the viscosity of the surrounding fluid and ρ_f the fluid's density. The timescale $\tau_f = \rho_f a^2/\eta$ estimates the time needed by the fluid vortex to propagate over the distance of one bead radius.

The characteristic time $\tau_p^* = m^*/6\pi\eta a$ corresponds to the momentum relaxation time by comparing the inertial forces with the stationary viscous drag. Ignoring the added mass due to the entrained fluid yields a time scale $\tau_p = m_p/6\pi\eta a$, and one readily calculates $\tau_p^* = \tau_p + \tau_f/9$. In a gas the distinction between τ_p and τ_p^* is unnecessary since the density of the gas is much smaller than the one of the particle. However, in a fluid the fluid and particle densities are often chosen to be comparable in order to prevent sedimentation. For the case of steady motion the well-known Stokes friction is recovered $\zeta(\omega = 0) = 6\pi\eta a$. The square root singularity in eqn (5) has to be evaluated with a positive real part, and introduces an algebraic long-time decay in $C(t)$. Consequently, a low-frequency series expansion of $\mathscr{Y}(\omega)$ and a subsequent analytic back transform into the temporal domain reveals

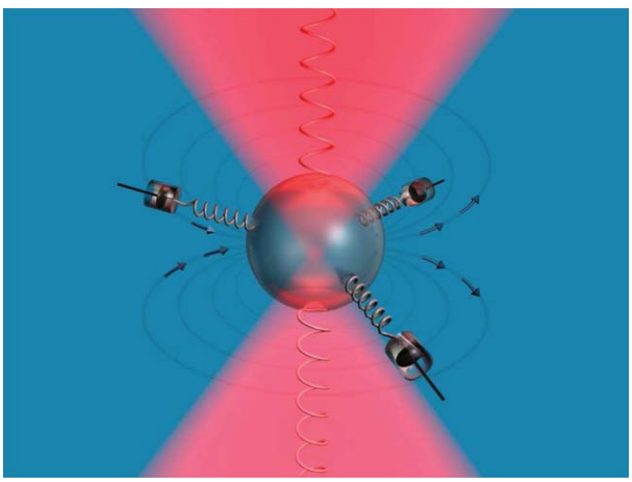

Fig. 1 Illustration of the investigated system. The viscoelastic fluid is typically represented by a dashpot and a spring connected in series to the Brownian particle. The dashpot mimics the viscous forces, whereas the spring stands for the elastic forces of the fluid acting on the Brownian sphere. The optical trap is also symbolized by a harmonic spring. The hydrodynamic backflow is shown as field lines developing around the bead.

the well-known $t^{-3/2}$ long-time tail in the VACF of a free particle. Its initial value is given by $C(t=0) = k_BT/m^*$ rather than $C(t=0) = k_BT/m_p$, which would follow from the equipartition theorem. The discrepancy can be traced back to the assumption of incompressibility of the fluid that ignores the rapid equilibration through sound modes.[39]

It is convenient to normalize the VACF to its initial value

$$\frac{C(t)}{C(0)} = \int_{-\infty}^{\infty} \frac{d\omega}{\pi} \mathrm{Re}[\mathscr{Y}_n(\omega)]\cos(\omega t), \tag{7}$$

introducing the normalized admittance $\mathscr{Y}_n(\omega) := m^*\mathscr{Y}(\omega)$. In order to observe Brownian motion experimentally over an extended period of time, the particle is typically held in an optical trap. Such confinement acts as an additional harmonic restoring force $F_{tr}(t) = -kx(t)$ on the bead, which can be readily accounted for in the admittance[18]

$$\mathscr{Y}_n(\omega) = \frac{m^*}{-i\omega m^* + \zeta(\omega) + k/(-i\omega)}. \tag{8}$$

Introducing the relaxation timescale of the harmonic potential $\tau_k = 6\pi\eta a/k$, the admittance can be expressed solely in terms of characteristic timescales

$$\mathscr{Y}_n(\omega) = \left[-i\omega + \frac{1+\sqrt{-i\omega\tau_f}}{\tau_p^*} + \frac{1}{-i\omega\tau_k\tau_p^*} \right]^{-1}. \tag{9}$$

A low-frequency expansion of the preceding equation reveals that the leading non-analytic term is of order $\omega^{5/2}$, which corresponds to a $t^{-7/2}$ long-time tail in the VACF.[40]

An alternative but equivalent characterization of Brownian motion in optical trapping is achieved in terms of the power spectral density (PSD)[41]

$$S(\omega) := \lim_{T\to\infty} \frac{1}{T}\left\langle |x_T(\omega)|^2 \right\rangle, \tag{10}$$

of the positional displacements with respect to the center of the trap. Here $x_T(\omega)$ represents the Fourier amplitudes of the displacement $x(t)$ from the center of the trap for a finite time window, $x_T(\omega) = \int_{-T/2}^{T/2} e^{i\omega t}x(t)dt$. As velocity is the time derivative of the positional displacement, the Wiener–Khinchin theorem provides the connection of the PSD to the VACF by $\omega^2 S(\omega) = \int_{-\infty}^{\infty} e^{i\omega t}\, C(t)dt$. Employing again the FDT of eqn (2), one finds for the PSD

$$S(\omega) = \frac{2k_BT}{\omega^2}\mathrm{Re}[\mathscr{Y}(\omega)]. \tag{11}$$

The MSD of an optically trapped particle connects then to the PSD by

$$\delta x^2(t) = \frac{2k_BT}{k} - \frac{2}{\pi}\int_0^{\infty} d\omega S(\omega)\cos(\omega t). \tag{12}$$

For long times, the particle equilibrates in the trap and by equipartition follows $\delta x^2(t\to\infty) = 2k_BT/k$.

3. Maxwell model

Complex solutions, like polymers or biological fluids, are usually composed of many different structures with sizes spanning several length scales. Therefore, their viscoelastic behavior displays significant deviations from a Newtonian fluid.[42,43] The simplest approach to describe viscoelasticity, already proposed by Maxwell in 1867, assumes that the material consists of a viscous element $\eta_0\dot{\gamma}$ and an elastic component $G_\infty\gamma$, with the zero-frequency viscosity η_0 and the elastic modulus G_∞, such that the shear rates add. Thus, the constitutive equation reads

$$\frac{1}{G_\infty}\dot{\sigma}(t) + \frac{1}{\eta_0}\sigma(t) = \dot{\gamma}(t). \tag{13}$$

A temporal Fourier transform, convention $f(\omega) := \int f(t)e^{i\omega t}dt$, readily relates the dynamic stress $\sigma(\omega) = G(\omega)\gamma(\omega)$ linearly to the dynamic strain $\gamma(\omega)$, where $G(\omega)$ is known as the complex elastic modulus. In the decomposition $G(\omega) = G'(\omega) - iG''(\omega)$, the real part $G'(\omega)$ refers to the storage modulus and the imaginary part $G''(\omega)$ to the loss modulus.[42,43] Since in equilibrium all systems are dissipative, the inequality $G''(\omega) \geq 0$ holds. Explicitly, for a Maxwell fluid one finds

$$G(\omega) = \frac{-i\omega\tau_M G_\infty}{1-i\omega\tau_M} = \frac{\omega^2\tau_M^2 G_\infty}{1+\omega^2\tau_M^2} - i\frac{\omega\tau_M G_\infty}{1+\omega^2\tau_M^2}, \tag{14}$$

where the Maxwell time τ_M characterizes the crossover from elastic to viscous behavior. Microscopically the dynamic viscosity is connected to the autocorrelation function of the fluctuating stress tensor by a Green–Kubo relation,[27] hence τ_M is the time scale where the structural relaxation of the solvent occurs. The spectral form of $G(\omega)$ corresponds to a simple Lorentzian. Equivalently, the dynamic stress $\sigma(\omega) = \eta(\omega)\dot{\gamma}(\omega)$ relates to the dynamic strain rate $\dot{\gamma}(\omega) = -i\omega\gamma(\omega)$ with a complex frequency-dependent viscosity $\eta(\omega) = G(\omega)/(-i\omega)$. Its real part is connected to the loss modulus *via* $\eta'(\omega) = G''(\omega)/\omega$ and its imaginary part to the storage modulus $\eta''(\omega) = G'(\omega)/\omega$.

The simplest version of the Maxwell model incorporates only the zero-frequency viscosity η_0 as dissipation mechanism. Yet,

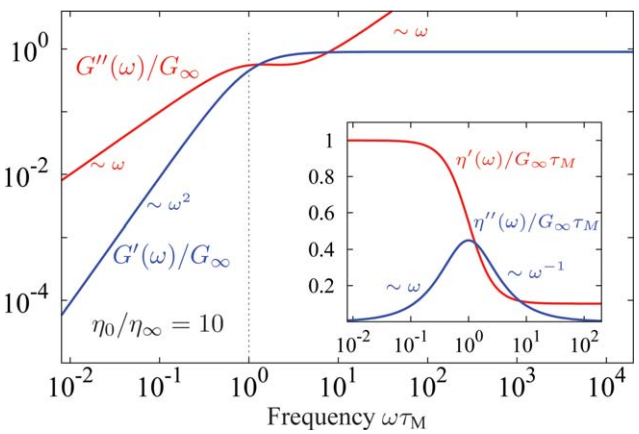

Fig. 2 Complex shear modulus $G(\omega) = G'(\omega) - iG''(\omega)$ as a function of angular frequency ω for a generalized Maxwell fluid. Parameters are chosen such that the stationary viscosity exceeds the background viscosity by a factor of $\eta_0/\eta_\infty = 10$. Inset: corresponding dynamic viscosity $\eta(\omega) = \eta'(\omega) + i\eta''(\omega)$.

typically the constituent mesoscopic particles in a viscoelastic material are immersed in a solvent giving rise to a background viscosity $\eta(\omega\to\infty)=\eta_\infty$. Hence to account for the dissipation in the solvent, we consider a generalized Maxwell model

$$\eta(\omega)=\eta_\infty+\frac{G_\infty\tau_M}{1-i\omega\tau_M}, \tag{15}$$

which is also known as Jeffreys' model.[44] In the following, the stationary shear viscosity will be denoted as $\eta_0=\eta(\omega=0)$. Fig. 2 shows the complex shear modulus and the corresponding frequency-dependent viscosity (inset) for a such a generalized Maxwell fluid. For frequencies $\omega\tau_M\ll 1$, the loss modulus $G''(\omega)$ dominates over the storage modulus indicative of viscous behavior. Similarly, at frequencies $\omega\gg G_\infty/\eta_\infty$ the fluid response is mainly viscous, here due to the background viscosity. In between, a window of frequencies opens, where the storage modulus $G'(\omega)$ dominates with the characteristic plateau G_∞, indicative of elastic behavior. The corresponding dynamic viscosity changes near $\omega\tau_M\approx 1$ from η_0 for small frequencies to the background viscosity η_∞.

When a microparticle is immersed in a viscoelastic fluid characterized by a dynamic, frequency-dependent viscosity $\eta(\omega)$, one readily calculates the dynamic Stokes drag on the immersed particle by solving the Navier–Stokes equations in the frequency domain with no-slip boundary condition and integrating over the stress tensor on the surface of the bead. All formulae introduced in Sec. 2, except eqn (9), remain valid provided the viscosity η is replaced by its frequency-dependent counterpart $\eta(\omega)$. The underlying assumption is that the frequency-dependent viscoelastic response entirely characterizes the motion of the bead. Yet, since the medium often displays structural heterogeneities at the mesoscale, boundary conditions are also crucial. In the context of polymeric networks, Maxwell's model has been generalized to a two-component fluid model, which allows the incorporation of different boundary conditions for the bead to the viscous and the elastic components.[45,46]

4. Free Brownian motion in a Maxwell fluid

In this section, we first recall briefly the effects of a Maxwell fluid on Brownian motion ignoring hydrodynamic memory. Next, we incorporate explicitly vortex diffusion and discuss the influence of the viscoelastic fluid on the VACF and the MSD of a Brownian particle in the absence of an external potential.

4.1. Instantaneous friction

The case of Brownian motion in a Maxwell fluid ignoring retardation effects and the background viscosity has already been discussed by van Zanten and Rufener.[29] We provide a generalization of their main results applying the theoretical framework introduced above on a Jeffreys' fluid. Here the frequency-dependent friction reduces to $\zeta(\omega)=6\pi\eta(\omega)a$, *i.e.* the frequency dependence is only inherited from the material properties of the fluid. This approximation is implicitly assumed in most experimental approaches to determine the complex elastic modulus.[5,13] Then the normalized admittance, eqn (4), reduces to

$$\mathscr{Y}_n(\omega)=\frac{m^*}{-i\omega m^*+6\pi\eta(\omega)a}. \tag{16}$$

Note that we keep the renormalization of the mass $m^*=m_p+m_f/2$ due to the entrained fluid. In the limit of a short Maxwell time, $\tau_M\to 0$ with G_∞ fixed, the fluid becomes purely viscous, $\eta(\omega)=\eta_\infty$, and the admittance exhibits a single pole on the negative imaginary axis. The corresponding VACF of the bead follows an exponential decay, $C(t)/C(0)=\exp(-t/\tau_p^*)$, which is just Langevin's description of viscously damped Brownian motion. Here and in the following $\tau_p^*=m^*/6\pi\eta_\infty a$ is defined with respect to the background viscosity.

In the general case $0<\tau_M<\infty$, the admittance exhibits two poles at complex frequencies $\omega=\pm\Omega-i\gamma$ with an oscillation frequency $\Omega^2=\omega_e^2-(1/\tau_M-1/\tau_p^*)^2/4$ and a damping constant $\gamma=1/2\tau_M+1/2\tau_p^*$. The medium's elastic response to the bead is described by the characteristic frequency $\omega_e^2=6\pi G_\infty a/m^*$. For weak damping the frequency Ω is real and results in a damped harmonic oscillator behavior of the VACF (Fig. 3, dashed line),

$$\frac{C(t)}{C(0)}=\left[\cos(\Omega t)+\frac{1}{2\Omega}\left(\frac{1}{\tau_M}-\frac{1}{\tau_p^*}\right)\sin(\Omega t)\right]e^{-\gamma t}. \tag{17}$$

In the limit of vanishing background viscosity $1/\tau_p^*\to 0$, this reduces to the solution of van Zanten and Rufener.[29]

An imaginary Ω leads to an overdamped oscillator behavior in the VACF:

$$\frac{C(t)}{C(0)}=\frac{1}{2|\Omega|}\left(\gamma_+-\frac{1}{\tau_p^*}\right)e^{-\gamma_- t}-\frac{1}{2|\Omega|}\left(\gamma_--\frac{1}{\tau_p^*}\right)e^{-\gamma_+ t}, \tag{18}$$

with decay rates $\gamma_\pm=\gamma\pm|\Omega|$. Overdamped behavior arises from either small Maxwell times $\tau_M<1/(1/\tau_p^*+2\omega_e)$ or large ones $\tau_M>1/(1/\tau_p^*-2\omega_e)$. If $\tau_M\ll\tau_p^*$, the fast decay rate $\gamma_+\approx 1/\tau_M$ reflects the mediums's structural relaxation, whereas the long time decay rate $\gamma_-\approx\omega_e^2\tau_M+1/\tau_p^*=6\pi\eta_0 a/m^*$ corresponds to viscous damping with the stationary viscosity η_0. In the opposite case $\tau_M\gg\tau_p^*$, the fast process transfers momentum to the fluid $\gamma_+\approx 1/\tau_p^*$, whereas inertia does not play a role in the slow decay any more. The rate $\gamma_-\approx\omega_e^2\tau_p^*+1/\tau_M=\eta_0/\eta_\infty\tau_M$ is only determined

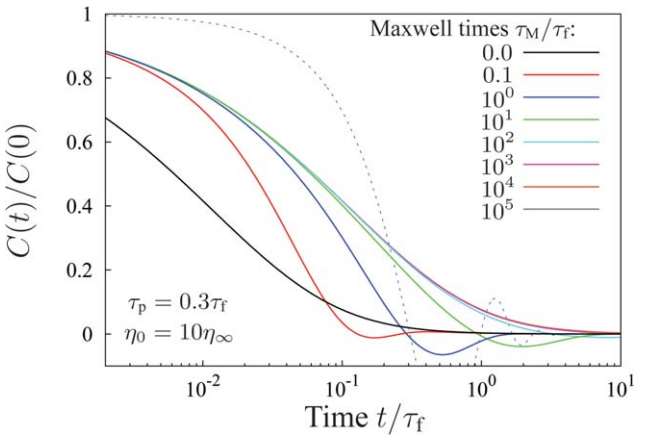

Fig. 3 Normalized VACF of a free particle in different Maxwell fluids. Maxwell times τ_M increase from left to right beginning with a simple fluid ($\tau_M=0$). The dashed line represents the VACF for $\tau_M=10\tau_f$ ignoring hydrodynamic interactions.

by the structural relaxation and the ratio of the low- and high-frequency viscosities.

4.2. Hydrodynamic memory

When vortex diffusion is taken into account, an analytic inverse Fourier transform of the admittance $\mathscr{Y}_n(\omega)$ is difficult to achieve due to the square root singularity in the friction

$$\zeta(\omega) = 6\pi\eta(\omega)a\left[1 + \sqrt{-i\omega\rho_f a^2/\eta(\omega)}\right]. \qquad (19)$$

Nevertheless, the limiting case of a purely viscous medium can be discussed analytically by performing a partial fraction decomposition in terms of the variable $\sqrt{s} := \sqrt{-i\omega}$. The corresponding VACF can then be represented by a superposition of error functions, as already discussed earlier.[21] The second limiting case that can be handled analytically is the purely elastic medium $\eta(\omega) = G_\infty/(-i\omega)$. There, the frequency-dependent friction becomes $\zeta(\omega)/m^* = \omega_e^2/(-i\omega) + \omega_e\sqrt{\tau_f/\tau_p^*}$ and acquires a real part, which implies dissipation (we define the vortex diffusion time with respect to the high-frequency viscosity, $\tau_f = \rho_f a^2/\eta_\infty$). This dissipation is due to the radiation of elastic shear waves that are generated by the oscillating spherical particle. Thus, for predominantly elastic materials radiation damping constitutes the principal mechanism of the VACF decay. The functional form of the time-dependent VACF corresponds then to a simple damped or even overdamped harmonic oscillator.

It is instructive to derive analytically the long-time behavior and the associated algebraic decay. As follows from the Tauber theorems,[47] a power-law long-time tail in the time domain is reflected in a corresponding low-frequency singularity in the Fourier transform. Assuming an asymptotic decay $C(t)/C(0) = a_x t^{-x}$ for $t \to \infty$ with some non-integer exponent x for the VACF, the admittance displays a leading low-frequency singularity

$$\mathscr{Y}(\omega) = a_x\Gamma(1 - x)(-i\omega)^{x-1} + \mathscr{O}(\omega^x) + \text{smooth}, \qquad (20)$$

superimposed on a smooth analytic background. The series expansion of $\mathscr{Y}(\omega)$ given by eqn (4), using the frequency-dependent friction $\zeta(\omega)$ of eqn (19) for the Maxwell model, reveals a leading non-analytic behavior of $\omega^{1/2}$. Comparison with eqn (20) yields a leading long-time anomaly in the VACF

$$C(t) = \frac{k_B T\sqrt{\rho_f}}{12\pi^{3/2}\eta_0^{3/2}} t^{-3/2}, \quad t \to \infty, \qquad (21)$$

which is identical to the one of a free particle in a simple fluid as discussed in Sec. 2. Note that only the stationary shear viscosity η_0 enters the expression. An elastic response of a Maxwell fluid is only expected for fast processes on timescales smaller than τ_M.

In the following, we discuss the experimentally relevant case of a polystyrene sphere in an aqueous viscoelastic medium with $\tau_p/\tau_f = 0.3$ ($\tau_p^*/\tau_f = 0.411$) and a background viscosity corresponding to water, $\eta_\infty = 10^{-3}$ Pa·s. However, it is then not obvious how analytic progress can be achieved. Therefore, we employ a numerical inverse Fourier transform based on a modified Filon algorithm,[48] which gives reliable results over many decades in time even in the presence of low-frequency singularities.[18] Furthermore, we use the generalized Maxwell model of eqn (15) and implicitly assume that the density of the fluid remains approximately constant as the viscoelasticity creating components are added to the aqueous solution. Such components can be for example worm-like micelles.

Usually the stationary viscosity η_0 can be obtained by macrorheological measurements and the high-frequency viscosity η_∞ corresponds to the one of the solvent. The experimental challenge is to infer the elastic modulus G_∞, respectively τ_M, from the data. Fig. 3 shows the normalized VACF for a free particle in Maxwell fluids for increasing τ_M as a function of t/τ_f assuming a fixed ratio $\eta_0/\eta_\infty = 10$, hence a fixed value for $G_\infty\tau_M$. For comparison, we also included the normalized VACF with the same parameters but for a Newtonian fluid where $\tau_M = 0$. The VACFs display, upon increase of τ_M, the appearance of anti-correlations, which are also detected in the VACF of an optically trapped particle in a simple viscous fluid.[17] Here, such anti-correlations originate from the restoring force of the elastic medium. As τ_M increases for a fixed η_∞, the fluid reacts more and more elastically, leading to pronounced minima in the VACF, which are most prominent for $\tau_M \approx \tau_f$. Since $G_\infty\tau_M$ is fixed, a further growing τ_M implies a decreasing value of the elastic modulus G_∞. Therefore, the minima in the VACF become shallower for higher τ_M scaling with $1/\tau_M$. When τ_M becomes much larger than τ_f, τ_p^*, while keeping the stationary viscosity η_0 fixed, the curves become insensitive to the detailed value of the Maxwell time. For comparison, we have included the VACF where vortex diffusion is ignored (dotted line in Fig. 3). The most striking difference is that then the VACF remains close to unity for times up to τ_p^*, whereas the coupling to hydrodynamics shows a significant decay already at much earlier times. Second, this curve oscillates much stronger with an infinite number of zeros. Thus the retarded friction renders the decay much more gradual and thereby strongly suppresses oscillations.

Fig. 4 displays five VACFs of Fig. 3 in a double logarithmic plot highlighting the zero-crossings. Indeed, the VACF in a generalized Maxwell fluid displays oscillations before reaching its long-time tail in contrast to a Newtonian fluid. Since all curves are for the same stationary viscosity η_0, all tails have the same

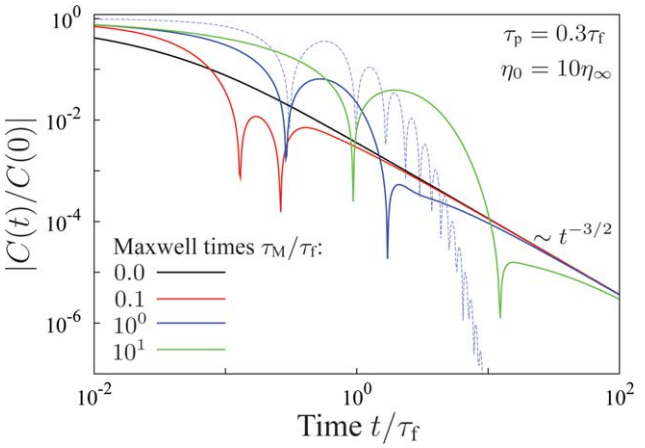

Fig. 4 Double logarithmic plot of three normalized VACFs of Fig. 3. This representation highlights the pairwise emergence of zero-crossings and the universal $t^{-3/2}$ long-time tail. The dashed line corresponds to a damped harmonic oscillator behavior.

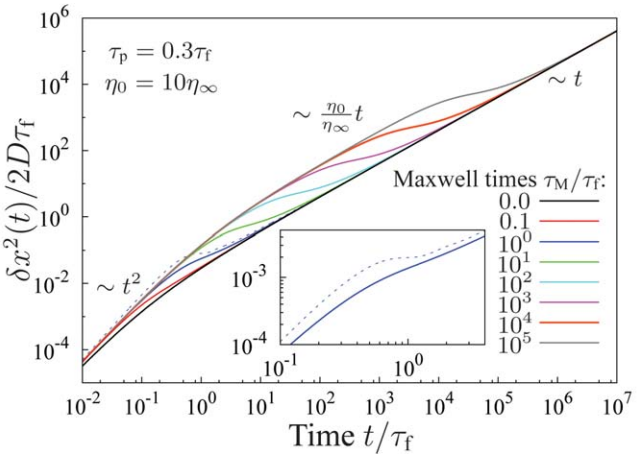

Fig. 5 Log–log plot of the mean-square displacements (MSD) corresponding to the VACF of Fig. 3. The Maxwell time τ_M increases from the lower right to the upper left. The dashed line corresponds to a MSD with $\tau_M = 10\tau_f$, where the influence of hydrodynamic backflow is ignored. Inset: zoom into the plateau region for $\tau_M = \tau_f$, highlighting the contribution of hydrodynamics.

amplitude, but the asymptote $t^{-3/2}$ is reached later for longer τ_M. Furthermore, zero-crossings shift to later times upon increase of τ_M. The effect of vortex diffusion is to constrain the number of nodes to a finite value. As the amplitude of the tail is positive, eqn (21), this number of zero-crossings has to be even. We observe only two zero-crossings in the experimentally relevant cases discussed here.

Most experiments in microrheology analyze the MSD of the bead, a quantity much less susceptible to noise than the VACF. To illustrate the role of the viscoelastic behavior, we have calculated the MSDs by integrating our numerical VACF, according to eqn (1). Since all Maxwell fluids are viscous at long times, the long-time behavior of the MSD is diffusive in all cases, and $\delta x^2(t) = 2Dt$ (Fig. 5) with the diffusion coefficient $D = k_BT/6\pi\eta_0 a$. For very short times $t \lesssim 0.1\tau_f$, the bead undergoes ballistic motion and the MSD grows quadratically $\delta x^2(t) = v^2t^2$, where $v^2 = k_BT/m^*$ corresponds to the thermal velocity. For Maxwell times τ_M large with respect to τ_p^* an additional diffusive regime emerges right after the ballistic growth. There, the particle's MSD increases linearly with $\delta x^2(t) = 2D_st$, where $D_s = k_BT/6\pi\eta_\infty a$ is the short-time diffusion coefficient determined by the viscosity of the solvent. Both diffusive asymptotes are connected by a crossover regime where the MSD grows subdiffusively due to the interplay with the structural relaxation of the fluid. This intermediate window terminates roughly at the Maxwell relaxation time τ_M. Similarly, the short-time diffusive behavior ends at an estimated time scale $\tau_M\eta_\infty/\eta_0$. For larger ratios η_0/η_∞ this crossover regime flattens and becomes a plateau at a value of the MSD at $2D\tau_M$ or $k_BT\tau_M/3\pi\eta_0 a$. Hence, in principle, one can directly extract the Maxwell time from the plateau of the MSD and G_∞ from the value of the long-time diffusion coefficient. For comparison, we have included the MSD ignoring the influence of hydrodynamic backflow in Fig. 5. Then, the crossover connecting the short and long-time diffusive regimes displays a more pronounced plateau (inset of Fig. 5). Thus, slow vortex diffusion smears out the transition giving rise to a more gradual increase of the MSD.

5. Trapped Brownian motion in a Maxwell fluid

Experiments monitoring the Brownian motion of a bead immersed in a complex fluid often rely on optical tweezers. The optical trap allows the observation of the particle over a long time interval, which greatly improves the statistical quality of collected data. The additional force acting on the Brownian particle can be approximated as a harmonic restoring force $F_{tr}(t) = -kx(t)$. Since even weak trapping modifies the long-time behavior of the correlation functions,[18] we include the effects of trapping in the following theoretical discussion.

As discussed in Sec. 2, the trap can be accounted for by using the admittance

$$\mathcal{Y}_n(\omega) = \frac{m^*}{-i\omega m^* + \zeta(\omega) + k/(-i\omega)}, \qquad (22)$$

where $\zeta(\omega)$ is given by eqn (19), and encodes the viscoelasticity *via* the frequency-dependent viscosity $\eta(\omega)$. For a Newtonian fluid, $\eta(\omega) = \eta_0 = \eta_\infty$, an analytic back transform in the temporal domain can be achieved[40] employing a partial fraction decomposition in the variable $\sqrt{s} = \sqrt{-i\omega}$, yet the complete expression requires the solution of a fourth order polynomial. In the limit of a purely elastic medium, $\eta(\omega) = G_\infty/(-i\omega)$, the normalized admittance simplifies to

$$\mathcal{Y}_n(\omega) = \frac{1}{-i\omega + \left(\omega_e^2 + \omega_k^2\right)/(-i\omega) + \omega_e\sqrt{\tau_f/\tau_p^*}}, \qquad (23)$$

where $\omega_k^2 = k/m^*$ is the characteristic harmonic oscillator frequency. Obviously, the elastic restoring force and the harmonic restoring force simply add, and the radiation of shear waves gives rise to new friction terms. The corresponding VACF exhibits again damped harmonic oscillations. Note that ignoring damping, the trapping and the elastic forces cannot be disentangled.

The general case of a viscoelastic medium has to rely again on a numerical Fourier back transform. Here, we choose a moderate trap with $\tau_k = 10^3\tau_f$, where $\tau_k := 6\pi\eta_0 a/k$ denotes the trap

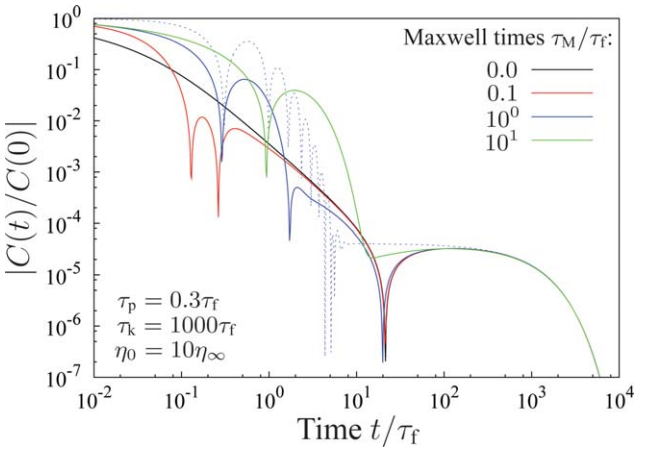

Fig. 6 Double logarithmic plot of the normalized VACFs of an optically trapped particle in different Maxwell fluids. The parameter $\tau_k = 1000\tau_f$ represents weak optical trapping. Maxwell times τ_M increase from left to right beginning with a simple fluid ($\tau_M = 0$). The dashed line corresponds to $\tau_M = 10\tau_f$ ignoring hydrodynamic backflow.

relaxation time. This definition of τ_k assumes that the relaxation in the trap occurs at times larger than τ_M such that the stationary viscosity η_0 determines the friction. For large Maxwell times, the dynamics induced by the trap precedes the structural relaxation and $\tau_{k,s} := 6\pi\eta_\infty a/k$ becomes the effective trapping time. For the chosen separation of time scales, $\tau_k \gg \tau_f$, the VACF on a linear y-axis is barely distinguishable from the free case (not shown). Nevetheless, it is instructive to display the VACFs on a log–log scale (Fig. 6) for the Maxwell fluids discussed in Fig. 3. Provided the timescale τ_k is well separated from τ_f and τ_p^* two regimes are clearly visble. When $\tau_M \lesssim \tau_k$ the motion is first dominated by the elastic restoring force of the fluid before the confinement of the trap sets in. When $\tau_M \gtrsim \tau_{k,s}$ the trapping dominates over the viscoelastic relaxation and the curves become insensitive to τ_M (not shown). For comparison, we have included in Fig. 6 the VACF of a particle immersed in a simple fluid showing the effect exclusively arising from the optical confinement at long times.

The manifestations of the trapping force become also clearly visible in the MSD. The most prominent feature is a saturation $\delta x^2(t\to\infty) = 2k_BT/k$ determined by the trapping force at long times. The MSDs normalized by their respective long-time limits are displayed in Fig. 7. After a diffusive increase of the MSD with the diffusion coefficient D_s, a similar intermediate plateau arises as already observed in Fig. 5. Before the MSD saturates due to trapping, a second diffusive regime with D is observed. Longer Maxwell times shift the intermediate plateau to higher values, eventually overlapping with the trap confinement at earlier times. The time interval for the beginning of the saturation is therefore comprised between $\tau_{k,s}$ and τ_k. Provided $\tau_M \lesssim \tau_k$, viscoelasticity does not interfere with trapping.

A complementary method to discuss Brownian motion is to consider the power spectrum of the particle's displacements in the trap. As mentioned in Sec. 2, the power spectral density $S(\omega)$ can be directly obtained from the admittance in eqn (11). The corresponding numerical results for $S(\omega)$ are displayed in Fig. 8 for increasing Maxwell times. For low frequencies the power spectrum saturates due to trapping at a value of $S(0) = 2k_BT\tau_k/k$, and the normalized power spectral density can be expressed as

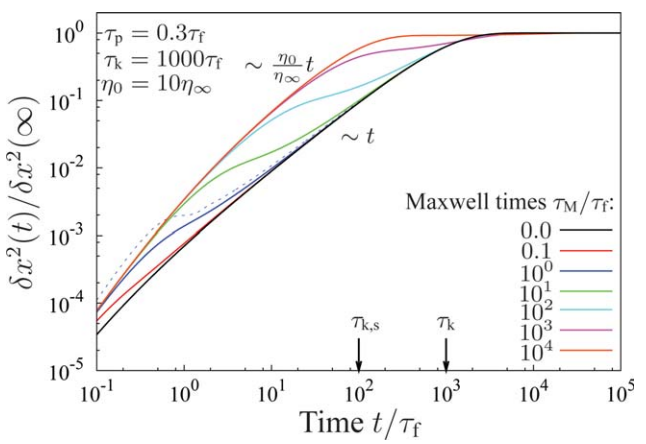

Fig. 7 MSD of an optically trapped Brownian particle. The MSDs are normalized to their long-time limit, $\delta x^2(t\to\infty) = 2k_BT/k$, resulting from optical trapping. Maxwell times rise from bottom to top beginning with a particle in a simple fluid ($\tau_M = 0$). The dashed line shows the MSD for $\tau_M = \tau_f$ calculated without hydrodynamic memory.

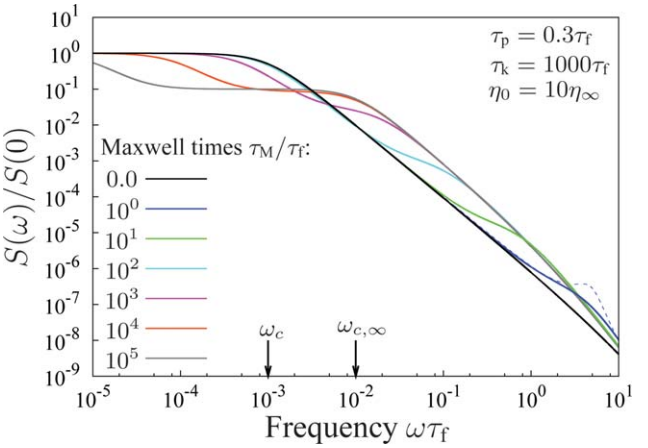

Fig. 8 Normalized PSDs of optically trapped particles in different Maxwell fluids. The Maxwell times rise from zero to $\tau_M = 10^5\tau_f$ from top to bottom. The dashed line corresponds to a PSD where hydrodynamic memory is ignored.

$$\frac{S(\omega)}{S(0)} = \frac{k^2}{6\pi\eta_0 a\omega^2}\,\frac{\zeta'(\omega)}{\left[m^*\omega - k/\omega - \zeta''(\omega)\right]^2 + \left[\zeta'(\omega)\right]^2}, \qquad (24)$$

where the frequency-dependent friction $\zeta(\omega) = \zeta'(\omega) + i\zeta''(\omega)$ is decomposed into its real and imaginary part. For reference, we have included in Fig. 8 the case of a Newtonian fluid, $\tau_M = 0$, where the most prominent feature is a decrease from the low-frequency plateau at the characteristic corner frequency $\omega_c = 1/\tau_k$. The power spectral densities for the Maxwell fluids differ drastically from this simple behavior in particular for large Maxwell times, *i.e.* the regime where the VACF and MSD are rather insensitive to the value of τ_M. The observed first decay from the low-frequency plateau is described by a Lorentzian $S(\omega)/S(0) = (1 - \eta_\infty/\eta_0)/[1 + (\omega\tau_M)^2] + \eta_\infty/\eta_0$. This follows from eqn (24) by neglecting all terms, except the trap restoring force in the denominator, $S(\omega)/S(0) \approx \zeta'(\omega)/6\pi\eta_0 a$, and ignoring the effects of the vortices in $\zeta'(\omega) \approx 6\pi\eta'(\omega)a$. The decay from the secondary plateau η_∞/η_0 reflects the trap relaxation and is well represented by another Lorentzian $S(\omega)/S(0) \approx (\eta_\infty/\eta_0)/[1 + (\omega\tau_{k,s})^2]$ with a corresponding short-time corner frequency $\omega_{c,\infty} = (\tau_{k,s})^{-1}$. For shorter Maxwell times $\tau_M \lesssim \tau_k$ the structural relaxation is superimposed on the trap relaxation process. Here, the decay of the PSD starts at the corner frequency ω_c. The intermediate plateaus already observed in the MSD (Fig. 7) are directly mirrored in the frequency domain. For the parameters studied here the effects of hydrodynamic backflow are negligible in the PSD (dashed blue line). However, for a significantly larger ratio η_0/η_∞ they give rise to new damping mechanisms such as radiation of shear waves.

6. Summary and conclusions

A bead performing Brownian motion in a viscoelastic medium can be employed to probe the material properties of the medium. This idea of a local reporter constitutes the basis of micro-rheology and has allowed the extraction of complex frequency-dependent elastic moduli by observing the thermally agitated motion of the bead in the sample. The approach is based on the

assumption that the solvent can be treated as a structureless homogenous continuum. Then, the coupling of the solvent's degrees of freedom to the bead is described by adopting suitable boundary conditions at the surface of the sphere. Such a description is certainly valid for large probe particles, but becomes questionable once the bead radius becomes comparable to the solvent's structural constituents.[34,49] Typically, complex materials are comprised of mesosized objects such as vesicles, micelles, transient or permanent polymer networks, and it remains an open question how the bead couples to this medium. Within the two-component fluid model, a generalization of Maxwell's model, different boundary conditions for the background solvent and the elastic network have been implemented and demonstrated to lead to sizable effects in the apparent complex elastic moduli.[45,46]

Most analysis of experimental data rely on the generalized Stokes–Einstein relation (GSE),[5,13] which translates in our notation to

$$GSE: \mathscr{Y}(\omega) = \frac{1}{6\pi\eta(\omega)a}, \tag{25}$$

i.e. the frequency-dependent mobility is essentially the inverse dynamic viscosity. In optical trapping measurements, which typically reach frequencies up to $1/\tau_p^*$, this expression has to be revised on several accounts. First, at low frequencies, trapping forces introduce an additional term, $k/(-i\omega)$, in the denominator. Second, at high frequencies, the inertia of the particle and the dragged fluid become important. These effects of hydrodynamic memory imply that dynamic friction is not simply proportional to the dynamic viscosity. The additional contribution arises from the slow diffusion of vortices excited by the thermal motion of the bead. Since this process is scale-free for a Newtonian fluid, its consequences are visible in the VACF over several decades in time.

Here, we exemplified the consequences of the interplay between hydrodynamic memory and viscoelastic properties of the medium for the case of a Maxwell fluid including the background viscosity of the solvent. First, we observed that the same long-time anomaly as in a Newtonian fluid is present in the Maxwell fluid, but becomes visible only at times larger than the Maxwell relaxation time. Second, when ignoring hydrodynamics, we showed that the effects of a purely elastic contribution in the dynamic viscosity cannot be distinguished from the harmonic restoring force of the optical trap. Furthermore, the coupling to degrees of freedom in the medium results in damping, even for a purely elastic medium, which arises from the excitation of shear waves by the particle. Depending on the values of the background viscosity, this mechanism may constitute the main source of friction.

The velocity autocorrelation function was identified as a sensitive quantity encoding the interplay of hydrodynamics and viscoelasticity. Its characteristic feature is a damped oscillatory behavior in response to medium elasticity. However, much fewer zero crossings than expected using the GSE appear. Furthermore, its decay is less steep and extends over several decades in time. Although analytic progress is possible, an accurate description was achieved only upon relying on a numerical Fourier transform.

The MSD is easier to obtain experimentally, since it is much less affected by noise. It is sensitive to the Maxwell relaxation time as an intermediate regime bridging the short-time to the long-time diffusion. The situation may be different for elastic moduli displaying essentially local power-law behavior, in which case the MSD of the bead also is governed by local power laws.[13] In the general viscoelastic case, it has been suggested recently to employ Padé approximants in the square-root of the frequency to extract the complex moduli.[26]

In the frequency domain, the power spectral density also encodes information on the viscoelastic behavior of the medium. Since the PSD involves the real and imaginary part of the dynamic viscosity, a direct separation of elastic and viscous contributions is not easily achievable. Yet, for well separated processes, it appears that the PSD is the quantity that is least sensitive to the effects of hydrodynamics. For example, the low-frequency singularity that leads to the long-time anomaly in the VACF is buried under a smooth background.

In this study, we focused on a scenario where the background viscosity and the stationary viscosity are known, and the high-frequency modulus G_∞ and the Maxwell time τ_M are the quantities to be determined experimentally. We demonstrated that the resulting curves display a series of features, which allow the measurement of these parameters accurately. As a consequence, high-frequency measurements in optical trapping constitute a sensitive tool to investigate structural relaxation processes in viscoelastic fluids with relaxation times from microseconds to hundreds of milliseconds.

7. Acknowledgements

We acknowledge helpful discussions with B. U. Felderhof and thank A. Doyon for drawing the illustration of Fig. 1. This work was supported by grants from the Swiss National Science Foundation through the NCCR-Nano module 1 and the project no. 200021-113529 to SJ and MG. MG is also supported by a scholarship of the German Academic Exchange Service (DAAD). TF acknowledges support by the German Excellence Initiative *via* the program 'Nanosystems Initiative Munich (NIM)'.

References

1 S. R. Derkach, *Adv. Colloid Interface Sci.*, 2009, **151**, 1.
2 D. Witz, *Annu. Rev. Biophys.*, 2009, **38**, 301.
3 T. M. Squires and T. G. Mason, *Annu. Rev. Fluid Mech.*, 2009, **42**, 413.
4 F. Gittes, B. Schnurr, P. D. Olmsted, F. C. MacKintosh and C. F. Schmidt, *Phys. Rev. Lett.*, 1997, **79**, 3286.
5 T. G. Mason, K. Ganesan, J. H. van Zanten, D. Wirtz and S. C. Kuo, *Phys. Rev. Lett.*, 1997, **79**, 3282.
6 J. Gagliano, M. Walb, B. Blaker, J. C. Macosko and G. Holzwarth, *Eur. Biophys. J.*, 2010, **39**, 801.
7 E. M. Furst, *Curr. Opin. Colloid Interface Sci.*, 2005, **10**, 79.
8 A. Yao, M. Tassieri, M. Padgett and J. Cooper, *Lab Chip*, 2009, **9**, 2568.
9 P. Cicuta and A. M. Donald, *Soft Matter*, 2007, **3**, 1449.
10 Y. Kimura, *J. Phys. Soc. Jpn.*, 2009, **78**, 041005.
11 C. Guzman, H. Flyvbjerg, R. Kőszali, C. Ecoffet, L. Forró and S. Jeney, *Appl. Phys. Lett.*, 2008, **93**, 184102.
12 E. Frey and K. Kroy, *Ann. Phys.*, 2005, **14**, 20.
13 T. G. Mason, *Rheol. Acta*, 2000, **39**, 371.
14 T. Gisler and D. A. Weitz, *Phys. Rev. Lett.*, 1999, **82**, 1606.
15 F. Gittes and C. F. Schmidt, *Opt. Lett.*, 1998, **23**, 7.

16 M. Atakhorrami, G. H. Koenderink, C. F. Schmidt and F. C. MacKintosh, *Phys. Rev. Lett.*, 2005, **95**, 208302.
17 S. Jeney, B. Lukić, J. A. Kraus, T. Franosch and L. Forró, *Phys. Rev. Lett.*, 2008, **100**, 240604.
18 T. Franosch and S. Jeney, *Phys. Rev. E: Stat., Nonlinear, Soft Matter Phys.*, 2009, **79**, 031402.
19 B. J. Alder and T. E. Wainwright, *Phys. Rev. Lett.*, 1967, **18**, 988.
20 V. Vladimirsky and Y. Terletzky, *Zhurnal Eksperimentalnoi i Teoreticheskoi Fiziki*, 1945, **15**, 258, in Russian, see V. Lisy, J. Tothova, arXiv:cond-mat/0410222 for a historic debate.
21 E. Hinch, *J. Fluid Mech.*, 1975, **72**, 499.
22 D. A. Weitz, D. J. Pine, P. N. Pusey and R. J. A. Tough, *Phys. Rev. Lett.*, 1989, **63**, 1747.
23 B. Lukić, S. Jeney, C. Tischer, A. J. Kulik, L. Forró and E.-L. Florin, *Phys. Rev. Lett.*, 2005, **95**, 160601.
24 B. Lukić, S. Jeney, Z. Sviben, A. J. Kulik, E.-L. Florin and L. Forró, *Phys. Rev. E: Stat., Nonlinear, Soft Matter Phys.*, 2007, **76**, 011112.
25 M. Atakhorrami, D. Mizuno, G. H. Koenderink, T. B. Liverpool, F. C. MacKintosh and C. F. Schmidt, *Phys. Rev. E: Stat., Nonlinear, Soft Matter Phys.*, 2008, **77**, 061508.
26 B. U. Felderhof, *J. Chem. Phys.*, 2009, **131**, 164904.
27 J. P. Boon and S. Yip, *Molecular Hydrodynamics* (Dover Publications, Inc., New York, 1991), reprint.
28 W. Götze, *Complex Dynamics of Glass-Forming Liquids – A Mode-Coupling Theory* (Oxford, 2009).
29 J. H. van Zanten and K. P. Rufener, *Phys. Rev. E: Stat. Phys., Plasmas, Fluids, Relat. Interdiscip. Top.*, 2000, **62**, 5389.
30 F. Cardinaux, L. Cipelletti, F. Scheffold and P. Schurtenberger, *Europhys. Lett.*, 2002, **57**, 738.
31 J. van der Gucht, N. A. M. Besseling, W. Knoben, L. Bouteiller and M. A. Cohen Stuart, *Phys. Rev. E: Stat. Phys., Plasmas, Fluids, Relat. Interdiscip. Top.*, 2003, **67**, 051106.
32 M. Buchanan, M. Atakhorrami, J. Palierne and C. F. Schmidt, *Macromolecules*, 2005, **38**, 8840.
33 J. Galvan-Miyoshi, J. Delgado and R. Castillo, *Eur. Phys. J. E*, 2008, **26**, 369.
34 J. Sprakel, J. van der Gucht, M. A. Cohen Stuart and N. A. M. Besseling, *Phys. Rev. E: Stat., Nonlinear, Soft Matter Phys.*, 2008, **77**, 061502.
35 R. Kubo, M. Toda, and N. Hashitsume, *Statistical Physics II, Nonequilibrium Statistical Mechanics,* (Springer, Berlin, Heidelberg, 1991).
36 J. Boussinesq, *C. R. Acad. Sci. Paris*, 1885, **100**, 935.
37 A. B. Basset, *Philos. Trans. R. Soc. London, Ser. A*, 1888, **179**, 43.
38 L. D. Landau and E. M. Lifschitz, *Fluid Mechanics, volume 6 of Course of Theoretical Physics* (Prentice-Hall, Oxford Pergamon Press, 1987), 2nd ed.
39 R. Zwanzig and M. Bixon, *Phys. Rev. A: At., Mol., Opt. Phys.*, 1970, **2**, 2005.
40 H. J. H. Clercx and P. P. J. M. Schram, *Phys. Rev. A: At., Mol., Opt. Phys.*, 1992, **46**, 1942.
41 K. Berg-Sørensen and H. Flyvbjerg, *Rev. Sci. Instrum.*, 2004, **75**, 594.
42 J. D. Ferry, *Viscoelastic Properties of Polymers* (John Wiley & Sons, New York, 1980).
43 R. Larson, *The structure and rheology of complex fluids* (Oxford University Press, Oxford, 1999).
44 H. Barnes, J. Hutton, and K. Walters, *An Introduction to Rheology* (Elsevier, Amsterdam, 1989), ISBN 0444871403.
45 M. Schmiedeberg and H. Stark, *Europhys. Lett.*, 2005, **69**, 629.
46 H. C. Fu, V. B. Shenoy and T. R. Powers, *Phys. Rev. E: Stat., Nonlinear, Soft Matter Phys.*, 2008, **78**, 061503.
47 W. Feller, *An Introduction to Probability Theory and Its Applications* (John Wiley & Sons, 1991).
48 E. Tuck, *Math, Comput*, 1967, **21**, 239.
49 J. Sprakel, J. van der Gucht, M. A. Cohen Stuart and N. A. M. Besseling, *Phys. Rev. Lett.*, 2007, **99**, 208301.

